Computer Fraud and Security
ISSN (online): 1873-7056

Cluster Partitioning Method for Distribution Networks with Distributed Photovoltaics Considering Voltage Stability

Shuqun Chen, Yongzhi Min*, Guo Wang, Weixi Lv, Haowen Chen
School of Automation and Electrical Engineering, Lanzhou Jiaotong University, Lanzhou 730070, Gansu, China.
**Corresponding Email:minyongzhi@lzjtu.edu.cn*

Abstract: To address the voltage stability degradation and increased topological complexity caused by the growing penetration of distributed photovoltaic systems in distribution networks, this paper proposes a voltage-stability-oriented cluster partitioning method. First, a comprehensive cluster partitioning index is established, considering both structural and functional aspects of the distribution network framework. Structurally, modularity metrics are used to quantify network aggregation characteristics, while functionally, dynamic evaluations integrate voltage stability indices and source-load matching indicators. Second, to overcome premature convergence in existing clustering algorithms, an improved coati optimization algorithm is proposed. This algorithm employs chaotic mapping for uniform population distribution, introduces adaptive escape operators to balance global exploration and local exploitation and incorporates optical opposition-based learning to enhance its ability to escape local optima. Finally, simulations on the IEEE 33-bus system demonstrate that the proposed comprehensive clustering index improves voltage stability by 46.79%, 49.54% and 47.83% compared to single indices, respectively. The improved clustering algorithm reduces computation time by 62.79% and 65.22% compared to the traditional coati algorithm and moth-flame optimization algorithm, while achieving 97.72% of centralized voltage control effectiveness with an 88.84% faster response time, verifying the effectiveness of the proposed method.

Keywords: Distribution network; Distributed photovoltaic; Cluster division; Improved coati optimization algorithm; Voltage stability index

INTRODUCTION

The increasing penetration of distributed photovoltaics (DPV) is transforming distribution networks from passive radial systems to active multi-agent collaborative architectures [1-2]. However, the inherent stochasticity and variability of high-penetration DPV integration exacerbate voltage fluctuations, particularly during local load trough periods, posing significant operational risks. Conventional control strategies primarily include localized control (offering fast response and low investment costs but limited regulation capacity) and centralized control (enabling global optimization but requiring substantial communication infrastructure investments) [3-4]. The emerging cluster-based control paradigm combines the advantages of both approaches through autonomous intra-cluster operation and inter-cluster coordination, providing an innovative solution for managing highly distributed PV integration [5].

Originating from complex network research, clustering theory has been progressively extended to distribution networks with distributed photovoltaic integration. Current clustering metrics primarily emphasize electrical coupling relationships between nodes within clusters, such as the modularity index that measures network structural strength-a metric originally developed for community detection in complex networks [6]. Additionally, scholars have proposed reactive power-voltage balance indices to assess intra-cluster voltage regulation capability from an operational control perspective, while other studies have introduced active power balance indices considering power complementarity characteristics within clusters to address renewable energy accommodation issues in planning [7-8]. In distribution network clustering algorithms, current approaches include coati optimization, bald eagle search, grey wolf optimization and more traditional optimization methods [9-11]. Reference [12] addresses dynamic electrical distance variations caused by wind power fluctuations by constructing a multi-scenario full-dimensional electrical distance matrix and using modified power flow state distance accumulation values as clustering criteria combined with hierarchical clustering techniques. Reference [13] innovatively establishes a three-dimensional evaluation system integrating electrical distance modularity with reactive/active power balance, implemented through an improved genetic algorithm. Reference [14] considers the

voltage regulation potential of PV inverters and energy storage devices to optimize cluster configurations using tabu search algorithms while simultaneously determining energy storage allocation. Reference [15] extracts electrical coupling characteristics during power transmission to construct a strength matrix, establishing a weighted network model combined with the fast Newman algorithm for grid clustering. Reference [16] reconstructs electrical distance calculation methods based on voltage sensitivity parameters, using modularity as the optimization objective and implementing reactive power-voltage clustering through an improved particle swarm optimization algorithm.

Existing clustering approaches predominantly rely on topological characteristics for network decomposition, fundamentally neglecting post-partition intra-zone voltage stability considerations and the dynamic coupling effects of voltage stability in functional dimensions, consequently resulting in inadequate source-load-storage coordination capability within partitioned regions and compromised voltage instability mitigation [17]. Specifically, current clustering metrics primarily focus on electrical coupling characteristics during the partitioning process or static performance indicators, failing to account for power distribution alterations induced by clustering, which ultimately undermines the ability to preserve voltage stability margins under variable generation-load scenarios [18-19]. Furthermore, prevailing algorithms exhibit two inherent limitations: traditional heuristic methods are prone to premature convergence and demonstrate limited adaptability to high-dimensional nonlinear optimization problems and conventional partitioning algorithms exhibit deficiencies in initial population diversity and convergence precision, leading to suboptimal performance in complex distribution network partitioning applications [20-21].

To overcome the key limitations of current clustering approaches in high-PV-penetration distribution networks - specifically their oversight of dynamic voltage stability and tendency toward premature convergence - this research develops a comprehensive framework combining a voltage-stability-focused clustering methodology with an enhanced coati optimization algorithm. The methodology utilizes a multi-criteria index assessing modularity, source-load matching and voltage stability margins to evaluate partition resilience during power fluctuations, facilitating simultaneous optimization of network topology and operational stability. The improved coati algorithm integrates chaotic initialization protocols, adaptive nonlinear search mechanisms and opposition-based refinement techniques to substantially enhance global exploration and solution precision. Extensive validation on a modified IEEE 33-bus test system confirms the framework's exceptional performance in delivering both superior clustering configurations and enhanced grid stability.

DISTRIBUTION NETWORK CLUSTER DIVISION INDEX SYSTEM

The proposed clustering index selection methodology adheres to both structural and functional principles. Structural considerations emphasize strong intra-cluster electrical coupling to ensure maximized connectivity within clusters and minimized inter-cluster connections, thereby maintaining appropriate cluster scales. Functional requirements prioritize enhanced power coordination between clusters and improved voltage stability within clusters, which fully leverages the renewable energy accommodation capacity and regulation characteristics of each partitioned zone.

1.1 Structural metrics

The modularity index, a classical metric for quantifying network community structures originally developed by Newman et al. and extended to weighted network partitioning, ranges from 0 to 1 [22]. Higher values indicate stronger functional similarity among intra-cluster nodes and weaker inter-cluster connections. In power distribution networks, edge weights can be defined using electrical distance parameters, where the modularity metric based on electrical coupling strength effectively evaluates structural aggregation characteristics in grid clustering. The time-period modularity index ρ_t is formulated as:

$$\rho_t = \frac{1}{m_t}\sum_i\sum_j (A_{ij,t} - \frac{k_{i,t}k_{j,t}}{m_t})\delta(i,j) \tag{1}$$

$$m_t = \sum_i\sum_j A_{ij,t} \tag{2}$$

$$\delta(i,j)=\begin{cases}1 & \text{Nodes } i \text{ and } j \text{ belong to the same cluster}\\ 0 & \text{Nodes } i \text{ and } j \text{ belong to different clusters}\end{cases} \tag{3}$$

where: m_t denotes the sum of all edge weights in the network during period t, equivalent to the summation of all elements in the edge weight matrix A; $A_{ij,t}$ represents the edge weight between nodes i and j during period t; $k_{i,t}$ is the sum of edge weights connected to node i during period t. This study defines edge weights based on electrical distance parameters, calculated via voltage-reactive power sensitivity relationships to quantify nodal electrical coupling strength. Specifically, electrical distance reflects the tightness of electrical coupling between nodes, expressed mathematically as:

$$\Delta V = S_{vQ}\Delta Q \tag{4}$$

where: S_{vQ} denotes the sensitivity matrix; ΔV and $\Delta \mathrm{Q}$ represent the voltage magnitude and reactive power variation vectors, respectively; The element $S_{VQ,ij}$ at row i and column j of matrix S_{VQ} quantifies the voltage variation at node i induced by a unit reactive power change at node j. It represents as:

$$d_{ij}=\lg\frac{S_{VQ,jj}}{S_{VQ,ij}} \tag{5}$$

where: d_{ij} represents the ratio of the voltage variation at node j to that at node i when the reactive power at node j changes, reflecting the degree of voltage influence exerted by node j on node i. A smaller value of d_{ij} indicates stronger electrical coupling between nodes i and j, corresponding to a shorter electrical distance.

In a power network, the relationship between any two nodes is not solely determined by themselves but is also influenced by the rest of the network. To account for the interconnected nature of nodal interactions, we define the electrical distance between node i and node j in an n-node system as:

$$A_{ij}=\sqrt{(d_{i1}-d_{j1})^2+(d_{i2}-d_{j2})^2+\cdots+(d_{in}-d_{jn})^2} \tag{6}$$

Given the time-varying impacts of load demand and generation output on electrical distances—and consequently on network partitioning results—this study adopts the average modularity index across all daily time periods as the final criterion for zone division:

$$\rho_{mean}=\sum_{t=1}^{T}\rho_t \tag{7}$$

where: the total number of time intervals T is set to 24.

1.2 Functional metrics

Functional metrics characterize the voltage regulation capability of controllable resources within clusters [23]. Post-partitioning, each cluster should achieve maximal self-governance to minimize inter-cluster power coordination losses. Traditional clustering relying solely on structural metrics only reflects nodal association strength through topological features, demonstrating clear limitations - particularly in renewable-penetrated grids where intra-zone energy autonomy must be ensured to reduce cross-regional power transmission losses and economic costs. Therefore, this study incorporates functional metrics including source-load matching degree and voltage stability indices into the clustering criteria.

(1) Source-Load Matching Index

The Source-Load Matching Index dynamically evaluates the spatiotemporal matching characteristics between regional photovoltaic generation and load demand. This metric advances beyond traditional static partitioning methods by establishing an assessment framework based on typical daily time-series scenarios. By analyzing the correspondence between 24-hour DPV output curves and load profiles, the morphological consistency of the two

sequences is quantified using cosine similarity algorithm. The index is defined as the cosine value of the two sequence vectors, expressed mathematically as:

$$M = \sum_{h=1}^{m} \frac{\sum_{t=1}^{24} x_{h,t} y_{h,t}}{\left(\sum_{t=1}^{24} x_{h,t}^2 \sum_{t=1}^{24} y_{h,t}^2 \right)^{\frac{1}{2}}} \tag{8}$$

where: m represents the number of clusters, $x_{h,t}$ and $y_{h,t}$ denote the aggregate DPV generation and total load demand, respectively, within cluster h at time t. When M approaches 1, curves x and y exhibit strong similarity. When M approaches 0, curves x and y show weak correlation.

(2) voltage stability index

The voltage stability index L is a static voltage stability assessment tool based on the feasible solution domain of branch voltage equations [24]. It can be rapidly calculated using local measurement data from phasor measurement units (PMUs). By constructing voltage-related branch equations and comprehensively considering key factors such as voltages at both ends of the branch, current, resistance, reactance, and voltage phase angle differences between nodes, the L_{pro} is derived. As an improvement over the L, the index eliminates interference from redundant measurement data, relying solely on PMU voltage measurements for computation, ensuring higher accuracy and linearity. Additionally, the L_{pro} remains applicable under three-phase asymmetric operating conditions, effectively evaluating voltage stability across various operational scenarios and demonstrating strong adaptability to complex real-world power systems. Whether in small-scale distribution networks or large interconnected grids, the L_{pro} provides consistent and reliable voltage stability assessments. This means power systems of different scales and topologies can adopt the same standard and method for voltage stability evaluation, offering an efficient and dependable tool for comparative analysis across different systems. The voltage stability index for branch ij during time interval t is expressed as:

$$L_{ij,t} = \frac{4[U_{i,t} U_{j,t} (\sin \delta_t + \cos \delta_t) - U_{j,t}^2]}{U_{i,t}^2 (1 + \sin 2\delta_t)} \tag{9}$$

where: $U_{i,t}$ and $U_{j,t}$ represent the per-unit voltage phasors at the sending-end node i and receiving-end node j of the branch during time interval t, respectively. δ_t denotes the voltage phase angle difference between the terminal nodes of the branch during time interval t.

When the voltage stability coefficient $L_{ij,t} \geq 1$, the distribution network system will experience significant voltage oscillations, ultimately leading to system instability. Given that voltage instability in a single line may trigger system-wide operational risks, this study adopts the maximum value $L_{pro,t}$ of the voltage stability parameters across all branches as the representation of the overall system voltage stability level during time interval t, defined mathematically as:

$$L_{pro,t} = \max_{ij \in S} \left\{ L_{ij,t} \right\} \tag{10}$$

where: S denotes the set of all system branches. The average system voltage stability index across all time intervals within a day is adopted as the final criterion for network partitioning, formulated as:

$$L_{mean} = \sum_{t=1}^{T} \frac{1}{m} \sum_{h=1}^{m} L_{pro,t,h} \tag{11}$$

where: $L_{pro,t,h}$ represents the voltage stability index of cluster h at time interval t.

MULTI-STRATEGY IMPROVED COATI OPTIMIZATION ALGORITHM

2.1 Coati optimization algorithm

The traditional Coati Optimization Algorithm (COA) simulates the cooperative attack of coatis on iguanas and their dispersed escape from predators [25]. It has the advantages of not requiring control parameter settings, high efficiency, strong balance, and powerful global exploration capabilities. Its principle is as follows:

(1) Exploration phase

The coati population N exhibits independent and stochastic spatial distribution X within the search space. The population implements a bifurcated search strategy: 50% of individuals simulate tree-climbing behavior to flush out prey (global exploration), while the remaining 50% maintain ground positions to capture randomly falling prey (local exploitation). The position update formula for arboreal coatis is given by:

$$X_{i,j}^{P1} = X_{i,j} + r(L_j - Ix_{i,j}) \tag{12}$$

Where: i denotes a coati individual within the population, j represents the problem dimension in the search space, L_j corresponds to the current global best position (gbest), γ signifies a uniform random number within the interval [0,1], I is a randomly selected integer from the discrete set $\{1,2\}$, implementing stochastic neighborhood sampling around gbest to simulate arboreal coati foraging behavior.

The positions of the iguanas after random dropping and the ground raccoons are represented by equations (13) and (14), respectively. The optimal position of the ground raccoons is updated based on the corresponding objective function value and the greedy strategy, as shown in equation (15).

$$L_j^G = b_j + r(a_j - b_j) \tag{13}$$

$$X_{i,j}^{\mathrm{P1}} = \begin{cases} X_{i,j} + r(L_j^{\mathrm{G}} - IX_{i,j}), & F_{L^G} < F_i \\ X_{i,j} + r(X_{i,j} - L_j^{\mathrm{G}}), & F_{L^G} > F_i \end{cases} \tag{14}$$

$$X_i = \begin{cases} X_i^{p1}, & F_i^{p1} < F_i \\ X_i, & F_i^{p1} > F_i \end{cases} \tag{15}$$

Where: a_j and b_j denote the upper and lower bounds, respectively, of the *j*-th dimension in the search space. γ represents a uniformly distributed random real number within the interval [0,1]. I is a randomly selected integer from the discrete set [1,2]. L_j^G corresponds to the position of the j iguana (prey) after a stochastic descent, with F_{L^G} being its associated objective function value. $X_{i,j}^{P_1}$ specifies the position of the i coati (search agent) in the *j*-th dimension, while F_i^{pl} evaluates its objective function value.

(2) Exploitation phase

When predators attack the coati population, the agents implement a dispersed escape strategy to avoid local optima entrapment. The position update during this defensive behavior is mathematically modeled as:

$$b_j^L = \frac{b_j}{t}, \quad a_j^{\mathrm{L}} = \frac{a_j}{t} \tag{16}$$

$$X_{i,j}^{\mathrm{P2}} = X_{i,j} + (1 - 2r)\left(b_j^{\mathrm{L}} + r(a_j^{\mathrm{L}} - b_j^{\mathrm{L}})\right) \tag{17}$$

Where: a_j^L, b_j^L denote the local upper bound and local lower bound of the *j*-th dimension, respectively. t is the number of iterations and the upper and lower bounds will be reduced with the number of iterations to simulate the local search ability of individual raccoons.; the optimal position is updated according to equation (18).

$$X_i = \begin{cases} X_i^{\mathrm{P2}}, & F_i^{\mathrm{P2}} < F_i \\ X_i, & F_i^{\mathrm{P2}} < F_i \end{cases} \tag{18}$$

2.2 Improved coati optimization algorithm

To address the standard COA's limitations of inadequate population diversity during initialization and susceptibility to local optima during exploitation, this study introduces three key enhancements: circle chaotic mapping for uniform population initialization, dynamic nonlinear escape strategy to prevent premature convergence and lens opposition-based learning to enhance global search capability. These modifications collectively form the Improved Coati Optimization Algorithm (ICOA).

(1) Circle chaotic mapping for population initialization

The circle chaotic mapping enhances the search space exploration range of the coati population while improving positional diversity. The circle map is defined as follows:

$$x_{t+1} = \mathrm{mod}\left(x_t + 0.2 - \frac{0.5}{2\pi}\sin(2\pi x_t), 1\right) \tag{19}$$

Where: *mod* denotes the modulo operation and t represents the iteration count.

(2) Dynamic nonlinear escape strategy

Building upon the energy consumption principle, this study introduces an adaptive factor with nonlinear adjustment to develop an innovative dynamic nonlinear escape strategy. This approach more accurately simulates coati escape behavior during the exploitation phase while maintaining adaptability to complex environments, enabling progressive emphasis on exploration during different escape stages. The adaptive factor $\alpha(t)$ is defined as:

$$\alpha(t) = \frac{2}{1 + e^{-\beta \cdot t}} - 1 \tag{20}$$

Where: β represents a hyperparameter, which is set to 0.6 in this study to enhance spatial search capability. The energy parameter is nonlinearly adjusted through a nonlinear function to simulate the dynamic energy consumption of coatis during escape, accounting for temporal and positional variations:

$$E' = E\left(1 - \varepsilon \cdot \tanh\left(\gamma t + \delta X_{i,j}\right)\right) \tag{21}$$

Where: E denotes the energy parameter for both coatis and predators, represented as a random number within [0,1]. E' represents the nonlinearly adjusted energy parameter. $\tanh$ is the arctangent function with a range of [-1,1]. γ and δ are parameters influencing temporal and spatial effects, respectively, both set to 0.5 to enhance local search capability. ε is the energy depletion coefficient, which linearly increases from 0 to 1 with iterations to simulate progressive energy decay, thereby gradually favoring local exploitation.

The coati's position during the exploitation phase is determined by equation (22)

$$\begin{cases} X_i^{P2} = X_{i,j} + \alpha(t) \cdot (1 - 2r \cdot (b_j^L + r \cdot (a_j^L - b_j^L))), & E_0' > E_1' \\ X_i^{P2} = X_{i,j} \cdot (2r - 1) \cdot |E_0' - E_1'|, & E_0' < E_1' \end{cases} \tag{22}$$

Where: $E_0^{'}$ and $E_1^{'}$ represent the adjusted energy parameters for the coati and predator, respectively.

(3) Lens opposition-based learning strategy

This strategy integrates opposition-based learning with lens imaging principles to generate inverse solutions relative to current coordinates, thereby expanding the search domain and progressively guiding the optimization toward the global optimum. The schematic diagram is illustrated in Figure 1.

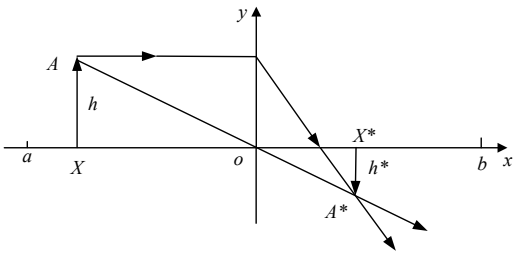

Fig.1 Schematic diagram of lens opposition-based learning

The search space range along the *x*-axis is defined as [a,b], while the *y*-axis represents the convex lens. Given an object *A* with *x*-axis projection *X* and height *h*, its optical image is formed through the convex lens. The resulting image A^* is formed at *x*-axis X^* with height h^*, yielding equation (23):

$$\frac{(a+b)/2-X}{X^*-(a+b)/2}=\frac{h}{h^*} \tag{23}$$

Where: $K=h/h^*$, parameters h is set to 1, while h^* linearly decreases with iterations to prioritize global exploration initially and local exploitation subsequently, thereby enhancing overall optimization performance.

The opposition solution is expressed as:

$$X_j^*=\frac{a_j+b_j}{2}+\frac{a_j+b_j-2X_j}{2K} \tag{24}$$

Where: X_j denotes the coati's position in the *j*-th dimension, X_j^* represents its opposition solution, while a_j and b_j specify the maximum and minimum boundaries of the *j*-th dimension respectively.

CLUSTER PARTITIONING MODEL FOR DISTRIBUTION NETWORKS WITH DISTRIBUTED PHOTOVOLTAICS

3.1 Objective function

The proposed clustering metric system coordinates structural characteristics with operational performance through three key indicators: modularity enhancement reflects improved topological aggregation, voltage stability coefficient reduction indicates increased security margins and source-load coordination improvement demonstrates enhanced supply-demand matching. The optimization model treats nodal cluster assignments as decision variables while incorporating: node parameters, branch connections and network topology features. The objective function minimizes the comprehensive clustering index:

$$\min f=w_1(1\text{-}\rho_{mean})+w_2(1-M)+w_3L_{mean} \tag{25}$$

Where: f denotes the objective function value, ω_1 , ω_2 and ω_3 represent the weighting coefficients for the modularity index, source-load matching index and voltage stability index, respectively.

The weighting coefficients for each metric are determined using the Analytic Hierarchy Process, which involves: constructing a judgment matrix and performing consistency validation [26]. Given the priority order modularity>source-load matching>voltage stability, the judgment matrix P is formulated as:

$$P=\begin{bmatrix} & \rho_{mean} & M & L_{mean} \\ \rho_{mean} & 1 & 3 & 5 \\ M & 1/3 & 1 & 3 \\ L_{mean} & 1/5 & 1/3 & 1 \end{bmatrix} \tag{26}$$

The calculated weighting coefficients are determined as $w_1=0.637$, $w_2=0.258$ and $w_3=0.105$ for each respective metric. Following consistency verification, the judgment matrix P achieves a random consistency

ratio of $CR = 0.0332 < 0.1$, thereby validating the rationality of the weight distribution among clustering evaluation indicators.

3.2 Constraints

To obtain the optimal clustering solution for distribution networks with distributed photovoltaics, the model incorporates the following constraints:

(1) Power flow constraints

$$\begin{cases} P_i = U_i \sum_{j=1}^{n} U_j \left(G_{ij} \cos\theta_{ij} + B_{ij} \sin\theta_{ij} \right) \\ Q_i = U_i \sum_{j=1}^{n} U_j \left(G_{ij} \sin\theta_{ij} - B_{ij} \cos\theta_{ij} \right) \end{cases} \tag{27}$$

Where: P_i and Q_i denote the active and reactive power at node i, respectively. G_{ij} and B_{ij} represent the conductance and susceptance between nodes i and j; θ_{ij} indicates the phase angle difference between nodes i and j.

(2) Power balance constraints

$$\sum_{i=1}^{N_{PCC}} P_{l,t}^{grid} + \sum_{c=1}^{N_\Omega} \sum_{i=1}^{N_C} P_{pv,i,t} = \sum_{c=1}^{N_\Omega} \sum_{i=1}^{N_C} P_{load,i,t} + \sum P_{ij,t}^{loss} \tag{28}$$

Where: N_{PCC}, N_Ω and N_C denote the number of branches connecting to the main grid, the total cluster count, and the node count within each cluster, respectively. $P_{l,t}^{grid}$, $P_{load,i,t}$ and $P_{ij,t}^{loss}$ represent the active power flow on upstream grid branch l, the load demand, and the active power loss on line ij at time t, respectively.

(3) Distribution network security constraints

$$\begin{cases} U_{\min} \le U \le U_{\max} \\ 0 \le I_{ij} \le I_{ij}^{\max} \end{cases} \tag{29}$$

Where: U represents the per-unit voltage magnitude of all nodes in the distribution system. I_{ij} denotes the branch current between nodes i and j. $I_{ij}^{\max}$ indicates the maximum allowable current for the branch connecting nodes i and j.

3.3 Cluster partitioning based on improved coati optimization algorithm

This study employs the multi-strategy improved coati optimization algorithm to solve the network partitioning problem, where the objective function-formulated using the comprehensive clustering index-serves as the fitness metric. The optimal partition corresponds to the solution with the minimal fitness value during iterative optimization. The complete algorithmic workflow is illustrated in Figure 2, comprising:

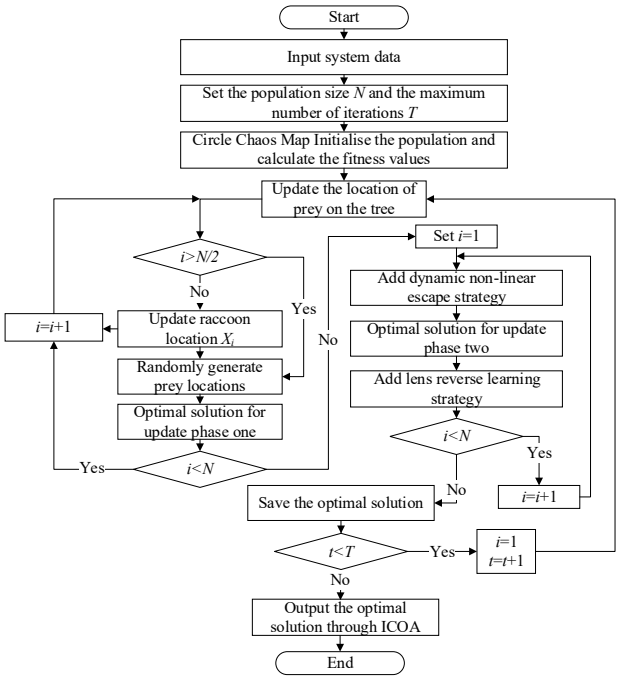

Fig.2 Flowchart of the ICOA-based cluster partitioning algorithm

RESULTS AND DISCUSSION

The improved IEEE 33-node system was analyzed using MATLAB 2016a, as shown in Figure 3.

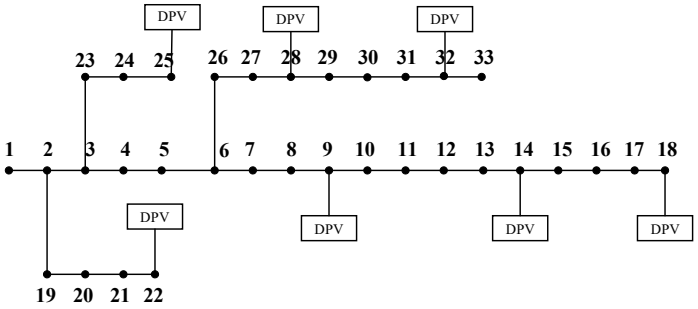

Fig.3 Improved IEEE 33-node system

The base capacity was set at 10 MW and the voltage level was 12.66 kV. Distributed photovoltaic (DPV) systems with a capacity of 500 kW were connected to nodes 9, 14, 18, 22, 25, 28 and 32. The load fluctuation curve and photovoltaic output are shown in Figure 4, respectively. The population size of the ICOA algorithm was set to N=50 and the maximum number of iterations was $T_{\max}=100$.

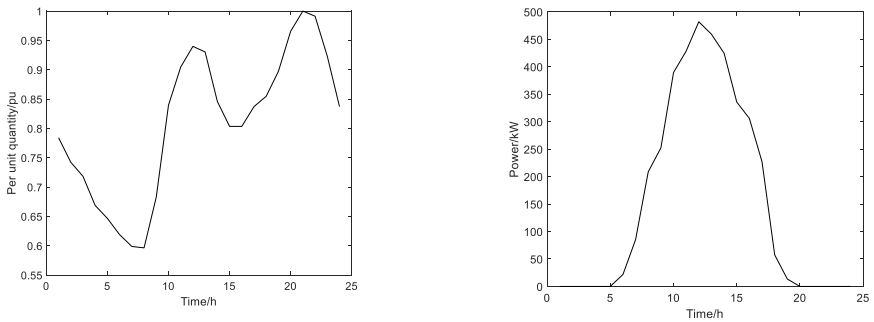

(a) (b)

Fig.4 Load and photovoltaic power curve: load output (a); photovoltaic output (b)

4.1 Effectiveness analysis of the proposed comprehensive index

To verify the effectiveness of the integrated clustering index, four comparative schemes are evaluated:

Scheme 1: Modularity index only;

Scheme 2: Source-load matching index only;

Scheme 3: Modularity index and source-load matching index;

Scheme 4: Proposed comprehensive index.

The performance results are summarized in Table 1.

Table.1 Comparative analysis of clustering metrics

Scheme	Modularity index	Source-load matching index	Voltage stability index	Cluster number
1	0.7531	0.8421	0.1357	3
2	0.6752	0.9413	0.1431	5
3	0.7354	0.9355	0.1384	4
4	0.7181	0.9206	0.0722	4

As demonstrated in Table 1: Scheme 1 achieves 11.54%, 2.41% and 4.87% higher modularity than alternative schemes respectively, while exhibiting significant deficiencies in other metrics. Similarly, Scheme 2 shows 11.78%, 0.62% and 2.25% superior source-load matching performance but demonstrates comparable limitations in remaining indices. Although Scheme 3 maintains balanced performance in both modularity and source-load matching without extreme cases, its elevated voltage stability index adversely affects system operational stability. In contrast, Scheme 4 not only preserves favorable structural characteristics but also significantly enhances both source-load matching and voltage stability, with the latter showing 46.79%, 49.54% and 47.83% improvements over Schemes 1-3 respectively. These results confirm the proposed comprehensive index's superior performance in network partitioning compared to single-metric approaches, while effectively mitigating voltage instability risks.The proposed comprehensive index demonstrates clear advantages over single-metric approaches by simultaneously ensuring topological cohesion, energy balance, and voltage security.

Figure 5 presents the cluster division diagrams for the four schemes:

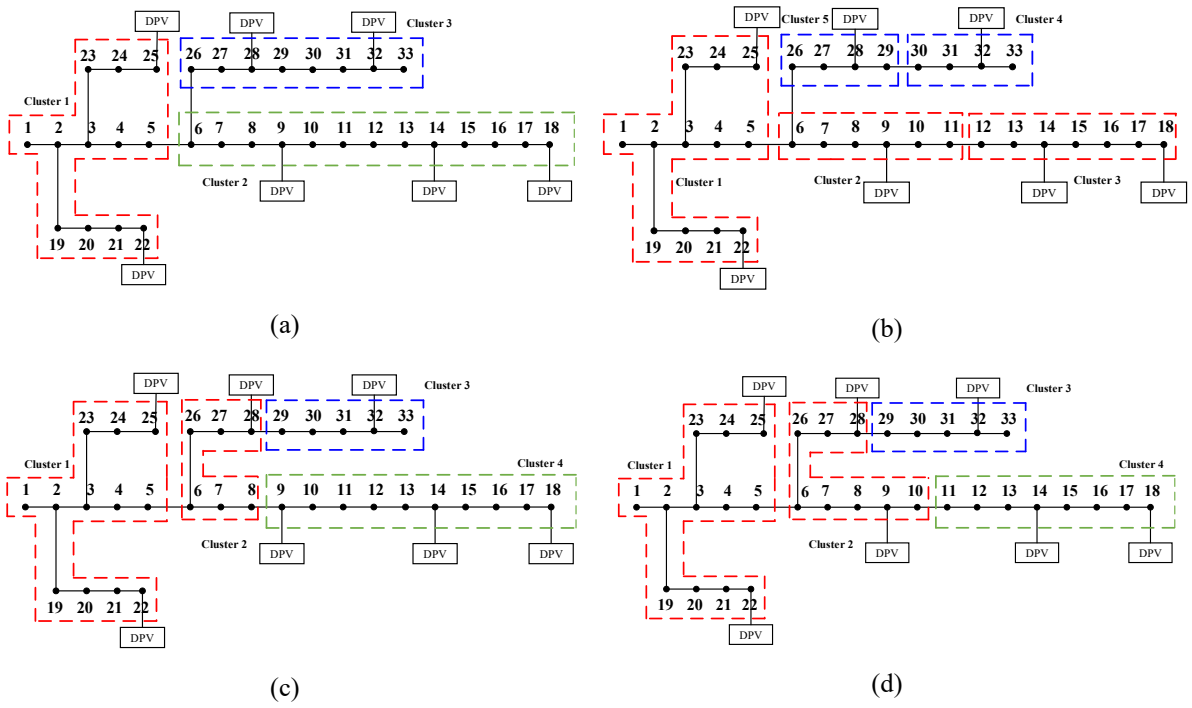

Fig.5 Cluster division result: scheme 1 (a); scheme 2 (b); scheme 3 (c); scheme 4 (d)

Figure 5 reveals that partitions generated using solely the modularity metric emphasize topological coupling strength between nodes, demonstrating superior structural aggregation characteristics, yet fail to incorporate source-load coordination considerations. When exclusively optimizing the source-load matching index, the inherent emphasis on supply-demand complementarity leads to reduced cluster counts and oversized single-region formations, significantly compromising structural integrity. The combined modularity and source-load matching approach maintains reasonable network architecture while improving spatiotemporal energy matching, though voltage stability margins remain suboptimal. Notably, the proposed comprehensive index exhibits differentiated configuration advantages, achieving balanced DPV capacity distribution across nodes. This configuration permits strategic nodal DPV capacities to moderately exceed local peak loads, establishing inter-cluster coordination that effectively enhances renewable energy accommodation capacity.

4.2 Comparative analysis of cluster partitioning algorithms

To verify the superiority of the proposed improved coati optimization algorithm for distribution network clustering, comparative analyses were conducted on a 33-node test system against conventional coati optimization algorithm (COA), moth-flame optimization algorithm (MFO), and particle swarm optimization algorithm (PSO). All four clustering algorithms employed the comprehensive clustering index proposed in this study, with their respective fitness convergence curves and optimization results presented in Figure 6 and Table 2.

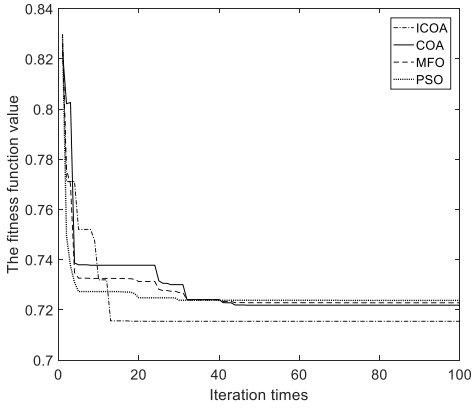

Fig.6 Fitness comparison curve

Table.2 Comparison of optimization algorithm metrics

Algorithm	Modularity index	Source-load matching index	Voltage stability index	Runtime/s
PSO	0.7018	0.9117	0.0785	134
MFO	0.7056	0.9141	0.0775	92
COA	0.7095	0.9179	0.0756	86
ICOA	0.7181	0.9206	0.0722	32

Figure 6 demonstrates that the COA exhibits premature convergence during later iterations due to gradual loss of population heterogeneity during evolutionary processes, while the proposed ICOA effectively maintains individual diversity in later stages through integrated dynamic nonlinear escape mechanisms and optical opposition-based learning strategies, thereby enhancing global search capability and significantly reducing the probability of local optima entrapment.

As evidenced in Table 2, the ICOA demonstrates superior optimization performance and stability compared to conventional methods. Specifically, the COA exhibits 1.10% and 0.68% improvements in modularity and source-load matching indices over PSO respectively, albeit with a 3.84% reduction in voltage stability. When compared to MFO, COA shows 0.55% and 0.42% enhancements in these metrics, accompanied by a 5.51% decrease in voltage stability. The proposed ICOA further outperforms COA with 1.21% and 0.29% increases in modularity and source-load matching, while maintaining comparable voltage stability (0.47% reduction). Notably, ICOA achieves significant computational efficiency gains, reducing runtime by 62.79%, 76.09% and 76.12% relative to

COA, MFO and PSO respectively. These results collectively demonstrate that the enhanced algorithm delivers both superior solution quality and accelerated convergence speed.

4.3 Comparison of the pressure regulation effects of different methods

The proposed clustering methodology establishes multiple DPV-dominated zones, effectively creating a novel multi-agent coordination framework for distributed energy resources that achieves dual objectives: maintaining strong intra-cluster nodal coupling while minimizing DPV-load power deviations through coordinated optimization. This approach enhances cluster-level autonomous regulation capability, improves regional self-sufficiency and reduces inter-area power exchange losses. For validation, three distinct clustering schemes were evaluated against centralized scheduling using daily total network loss, voltage deviation, and stability as optimization targets: Scheme A (modularity-only), Scheme B (modularity+source-load matching) and Scheme C (comprehensive modularity+source-load matching+voltage stability index).

The comparison curves of the three performance indicators are shown in Figure 7:

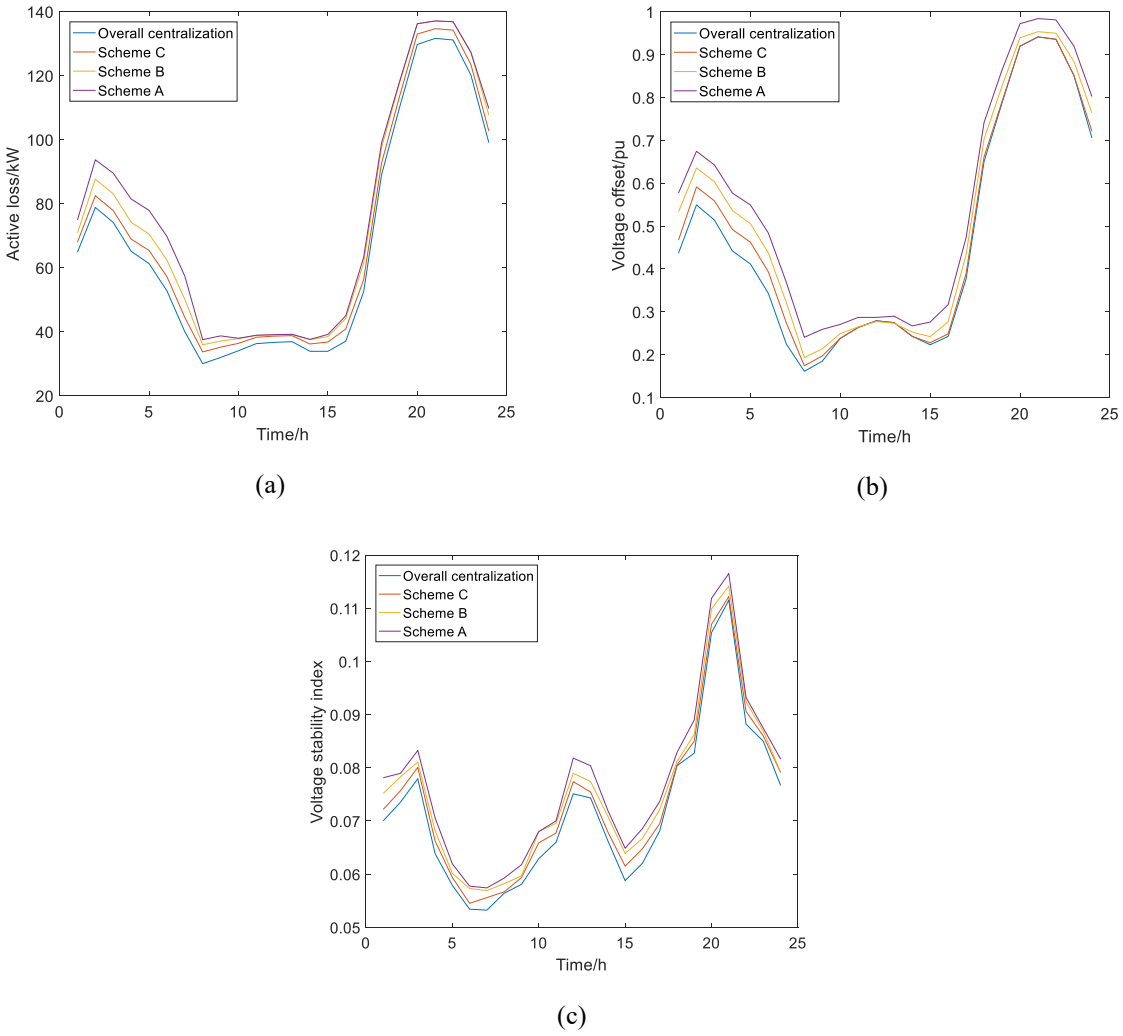

Fig.7 Comparison curve of operation index: network loss comparison curve (a); voltage offset comparison curve (b); voltage stability index comparison curve (c)

Figure 7 demonstrates that while clustered architectures generally exhibit inferior operational metrics compared to centralized systems, the proposed enhanced clustering framework - incorporating modularity, voltage stability, and source-load matching indices - shows significant performance improvements across all indicators. Experimental results reveal a computational accuracy of 97.72%, with merely 2.28% deviation from the

centralized scheduling benchmark, confirming that the clustered scheduling mechanism achieves near-equivalent optimization efficacy to centralized approaches and validates its practical applicability in power system operations.

The implementation of the clustered scheduling paradigm reduces computational time by 88.84% compared to centralized approaches, achieved through partitioning the integrated system into multiple autonomous sub-units that constrain information retrieval to specific regional domains rather than network-wide analysis, thereby significantly optimizing scheduling efficiency.

The comparison of optimization results are detailed in Table 3.

Table.3 Comparison of optimization results

Scheme	Total daily active power loss/kW	Daily voltage deviation/pu	Daily voltage stability index	Optimize time/s
A	1.8246e+03	13.1037	1.8511	1.81
B	1.7679e+03	12.2692	1.8125	1.95
C	1.6888e+03	11.5940	1.7703	1.76
Overall centralized	1.6103e+03	11.1994	1.7280	15.77

Table 3 reveals Scheme A's suboptimal performance stemming from its sole dependence on modularity metrics that capture topological connectivity but disregard regional supply-demand equilibrium. This approach leads to clusters requiring external power transactions due to energy insufficiency and induces system losses through compensatory power flows caused by significant PV-load imbalances. Conversely, Schemes B and C demonstrate markedly enhanced operational characteristics by integrating source-load matching metrics that strengthen intra-cluster coordination and optimize spatiotemporal energy distribution for maximal regional self-sufficiency. Scheme C's incorporation of voltage stability metrics provides additional refinement by emphasizing autonomous stable operation, effectively reducing external power dependencies while preserving robust security thresholds.

CONCLUSION

To address voltage stability deterioration and topological complexity in distribution networks with high-penetration distributed photovoltaics, this study proposes a comprehensive clustering index incorporating both structural and functional characteristics, implemented through the ICOA algorithm, yielding the following key findings:

(1) The integrated clustering index combining modularity, source-load matching and voltage stability demonstrates superior performance compared to single-metric approaches by simultaneously addressing both structural and functional requirements, effectively mitigating voltage instability risks and confirming the validity of the proposed comprehensive evaluation framework.

(2) The proposed ICOA algorithm, incorporating dynamic nonlinear escape strategies and lens opposition-based learning mechanisms, effectively addresses the limitations of conventional clustering methods. Post-partition analysis confirms the algorithm's capability to maintain network connectivity without isolated nodes while demonstrating superior computational efficiency and enhanced global search capabilities in distribution system applications.

(3) The implemented clustering framework demonstrates significant improvements, achieving 46.79%, 49.54% and 47.83% voltage stability enhancements compared to single-metric approaches, while reducing computational time by 62.79%, 76.09% and 76.12% relative to COA, MFO and PSO algorithms respectively. The voltage regulation efficacy reaches 97.72% of centralized control performance with an 88.84% response time improvement, conclusively validating the feasibility of both the comprehensive index and optimization algorithm.

ACKNOWLEDGEMENT

This project supported by the National Natural Science Foundation of China (NO.52467007).

REFRENCES

[1] Sun, X., & Jing, Q. (2021). Hierarchical voltage control strategy in distribution networks considering customized charging navigation of electric vehicles. *IEEE Transactions on Smart Grid*, 12(6), 4752-4764.

[2] Gonzalez-Sotres. L., Pablo, F., & Carlos, M. (2017). Techno-economic assessment of forecasting and communication on centralized voltage control with high PV penetration. *Electric Power Systems Research*, 151: 338-347.

[3] Xu, X., Li, Y., Yan, Z., Ma, H., & Mohammad, S. (2022). Hierarchical central-local inverter-based voltage control in distribution networks considering stochastic PV power admissible range. *IEEE Transactions on Smart Grid*, 14(3), 1868-1879.

[4] Ji, H., Wang., Li, Peng., Zhao, J., Song, G., Ding, F., & Wu, J. (2018). A centralized-based method to determine the local voltage control strategies of distributed generator operation in active distribution networks. *Applied energy*, 228: 2024-2036.

[5] Chai, Y., Li, G., Wang, C, Zhao, Z., Du, X., & Pan J. (2018). Network partition and voltage coordination control for distribution networks with high penetration of distributed PV units. *IEEE Transactions on Power Systems*, 33(3), 3396-3407.

[6] Li, P., Zhang, C., Wu, Z., Xu, Y., Hu, M., & Dong, Z. (2019). Distributed adaptive robust voltage/var control with network partition in active distribution networks. *IEEE Transactions on Smart Grid*, 11(3), 2245-2256.

[7] Su, S., Lei, J., Yan, Y., Pan, S., Yang, Y., Bai, H., Li, W., Chen, J., & Zhao, Q. (2023). Voltage regulation strategy of distribution network with decentralized wind power based on cluster partition. *Recent Advances in Electrical & Electronic Engineering (Formerly Recent Patents on Electrical & Electronic Engineering)*, 16(1), 30-44.

[8] Bahramipanah, M., Rachid, C., & Mario, P. (2016). Decentralized voltage control of clustered active distribution network by means of energy storage systems. *Electric Power Systems Research*, 136: 370-382.

[9] Nguyen, T., & Hak-Man, K. (2020). Cluster-based predictive PCC voltage control of large-scale offshore wind farm. *IEEE Access* 9: 4630-4641.

[10] Sheng, H., Wu, Q., Zhao, J., & Liao, W. (2019). Distributed optimal voltage control for VSC-HVDC connected large-scale wind farm cluster based on analytical target cascading method. *IEEE Transactions on Sustainable Energy*, 11(4), 2152-2161.

[11] Zhang, H., Peng, M., & Peter, P. (2019). Intentional islanding method based on community detection for distribution networks. *IET Generation, Transmission & Distribution*, 13(1), 30-36.

[12] Hu, J., Zhou, H., Li, Y., Hou, P., & Yang, G. (2020). Multi-time scale energy management strategy of aggregator characterized by photovoltaic generation and electric vehicles. *Journal of Modern Power Systems and Clean Energy*, 8(4), 727-736.

[13] Abessi, A., Vahid, V., & Mohammad, S, G. (2015). Centralized support distributed voltage control by using end-users as reactive power support. *IEEE Transactions on Smart Grid*, 7(1), 178-188.

[14] Nayeripour, M., Hossein, F., Eberhard, W., & Saeed, H. (2016). Coordinated online voltage management of distributed generation using network partitioning. *Electric Power Systems Research* 141: 202-209.

[15] Ali. A., Keerio, M, U., & Laghari, J, A. (2020). Optimal site and size of distributed generation allocation in radial distribution network using multi-objective optimization. *Journal of Modern Power Systems and Clean Energy*, 9(2), 404-415.

[16] Aolaritei, L., Saverio, B., & Florian, D. (2018). Hierarchical and distributed monitoring of voltage stability in distribution networks. *IEEE Transactions on Power Systems*, 33(6), 6705-6714.

[17] Wang, W., & Keyi, K. (2024). Research on energy storage capacity optimization of rural household photovoltaic system considering energy storage sharing. *Environmental Science and Pollution Research*, 31(34), 47084-47100.

[18] Wang, J., Xu, W., Gu, Y., Song, W., & Tim, C, G. (2021). Multi-agent reinforcement learning for active voltage control on power distribution networks. *Advances in Neural Information Processing Systems*, 34: 3271-3284.

[19] Dall, A., Emiliano, S, D., & Georgios, B, G. (2014). Optimal dispatch of photovoltaic inverters in residential distribution systems. *IEEE Transactions on Sustainable Energy*, 5(2), 487-497.

[20] Wang, Z., Wang, Y., Liu, G., Zhao, Y., Cheng, Q., & Wang, C. (2020). Fast distributed voltage control for PV generation clusters based on approximate newton method. *IEEE Transactions on Sustainable Energy*, 12(1), 612-622.

[21] Procopiou., Andreas, T., & Luis, F, O. (2016). Voltage control in PV-rich LV networks without remote monitoring. *IEEE transactions on power systems*, 32(2), 1224-1236.

[22] Girvan, M., & Mark, E, N. (2002). Community structure in social and biological networks. *Proceedings of the national academy of sciences*, 99(12), 7821-7826.

[23] Alyami, S., Wang, Y., Wang, Caisheng., Zhao, J., & Zhao, Bo. (2014). Adaptive real power capping method for fair overvoltage regulation of distribution networks with high penetration of PV systems. *IEEE Transactions on Smart Grid*, 5(6), 2729-2738.

[24] Nguyen, T., & Hak-Man, K. (2020). Cluster-based predictive PCC voltage control of large-scale offshore wind farm. *IEEE Access* 9: 4630-4641.

[25] Sun, F., Ma, J., Yu, Miao., & Wei, W. (2019). A robust optimal coordinated droop control method for multiple VSCs in AC–DC distribution network. *IEEE Transactions on Power Systems*, 34(6), 5002-5011.

[26] Li, P., Wu, Z., Zhang, C., Xu, Yan., Dong, Z., & Hu, M. (2021). Multi-timescale affinely adjustable robust reactive power dispatch of distribution networks integrated with high penetration of PV. *Journal of Modern Power Systems and Clean Energy*, 11(1), 324-334.